BOUNDS ON INTERGALACTIC COMPACT OBJECTS FROM OBSERVATIONS OF COMPACT RADIO SOURCES

AGGELIKI KASSIOLA¹ AND ISRAEL KOVNER²
Physics Department, The Weizmann Institute of Science, Rehovot 76100, Israel

AND

ROGER D. BLANDFORD

Theoretical Astrophysics, California Institute of Technology, Pasadena, CA 91125 Received 1990 October 29; accepted 1991 May 13

ABSTRACT

We investigate the constraints that can be imposed on the cosmic density of uniformly distributed intergalactic compact objects in the mass range $10^7 \lesssim M/M_\odot \lesssim 10^9$ using VLBI observations of compact radio sources. A compact object at a sufficiently small angular separation from a compact radio source produces a deamplified and inverted secondary image. No such cases are known. Using published maps of compact radio sources and assuming an Einstein-de Sitter cosmology, we exclude a density parameter for mass in this range $\Omega_M > 0.4$ at the 99.7% confidence level. Observations using the VLBA should allow one to exclude or discover $\Omega_M \gtrsim 10^{-3}$ for compact objects in the mass range $10^5 \lesssim M/M_\odot \lesssim 10^8$.

Subject headings: cosmology — galaxies: intergalactic medium — gravitational lenses — radio sources: galaxies

1. INTRODUCTION

Press & Gunn (1973) first investigated in detail the effect that intergalactic compact objects would produce on distant quasars. They showed that observations of radio quasars could be useful for ruling out a cosmologically significant density of objects of mass $\gtrsim 10^6 M_{\odot}$. Subsequently, Canizares (1982) used the small observed variation in line equivalent widths in quasar spectra to exclude a closure density of compact objects in the range $10^{-2} < M/M_{\odot} < 10^{5}$. In addition, Blandford & Jaroszyński (1981) considered the distortion of linear radio sources by clusters of galaxies and Hewitt et al. (1989) gave preliminary results on bounds on compact objects of $M/M_{\odot} \sim 10^{11}$ - 10^{12} from a VLA survey. More recently, J. N. Hewitt and M. V. Gorenstein (private communication) have used the Mark III VLBI archive to set limits on the incidence of secondary images on the angular scale $\sim 0.2-5$, and Nemiroff (1991) has derived limits for compact objects more massive than $10^{10} M_{\odot}$.

In this paper we use VLBI data on compact radio sources to constrain the density of intergalactic compact masses. Many of these sources are superluminal and an intervening compact object would create an inverted secondary image in the field, of reduced size and, consequently, of reduced expansion speed. Observers would not have failed to notice such a phenomenon and no such example has been reported. (Conversely, gravitational lensing has been used by some to interpret superluminal sources, e.g., Barnothy 1982; Ostriker & Vietri 1985. However, we take the view that the absence of apparent multiple imaging in the maps provides a strong argument against gravitational magnification.)

The organization of the paper is as follows: In § 2 we review very briefly the lensing properties of a point mass. In § 3 we derive the probability of nondetection for a point-mass lens in front of a point source. This derivation is valid for an isolated

lens and does not take into account the existence of other lenses in the universe; a different approach to the problem, which accounts for this effect, is outlined in § 4. We use existing observations to derive an upper limit on the compact object density in § 5 and briefly discuss our conclusions in § 6.

2. LENSING PROPERTIES OF A POINT MASS

The point-mass lens has been extensively studied in the literature; here we shall briefly review some of its properties.

We trace rays back from the observer, and consider (in the small angle approximation) projections of unit vectors aligned with the rays on a plane perpendicular to some (arbitrary) axis: $\mathbf{r} = (x, y)$ are angular coordinates of an image in the "image plane," while $\mathbf{s} = (s_x, s_y)$ are angular coordinates of a source point in the "source plane." The magnification of a small source is $A = [\det(\partial s_i/\partial r_j)]^{-1} (A < 0)$ for inverted images. The image position can be found from the lens equation, $\mathbf{s} = \mathbf{r} - \nabla \Phi(\mathbf{r})$, where $\Phi(\mathbf{r})$ is the two-dimensional dimensionless (effective) lens potential.

For a point mass M on the axis, the lens potential is $\Phi(r) = E^2 \ln r$, where E is the Einstein radius: A small source on the axis would be observed as a ring of radius E, given by the relation

$$E^2 = \frac{4MG}{c^2} \frac{d_{1s}}{d_{01}d_{0s}}, \qquad (1)$$

where d_{os} , d_{ol} , and d_{ls} are the observer-source, observer-lens, and lens-source angular diameter distances, respectively. Therefore, for $s = (s_x, 0)$, the lens equation is

$$s_x = x - E^2/x . (2)$$

Let us rewrite it as

$$x^2 - s_x x - E^2 = 0. (3)$$

Then the positions of the two images are related by

$$x_1 x_2 = -E^2 \,, \tag{4}$$

so that one image is located outside the Einstein ring with

On leave from Observatoire Midi-Pyrennees.

² Incumbent of the Charles H. Revson Foundation Career Development Chair.

 $x_1 > E$, and the other within the ring $x_2 < E$. Their magnifications A satisfy

$$A = (1 - E^4/r^4)^{-1} . (5)$$

The outer image has positive parity with $A_1 > 1$, and the inner image is inverted with $A_2 < 0$. As the distance s of the source from the optic axis is increased, the magnification of the outer image approaches unity and that of the inner, inverted image diminishes to zero. If the compact object is a black hole, there will always be a second image. However, it will only be observable for small enough values of s.

The ratio of the two magnifications is

$$R = \left| \frac{A_1}{A_2} \right| = \left| \frac{1 - E^4 / x_2^4}{1 - E^4 / x_1^4} \right| = \left| \frac{x_1}{E} \right|^4, \tag{6}$$

where equation (4) was used. This gives immediately the position of the brighter image

$$x_1 = ER^{1/4} \tag{7}$$

and the source-lens angular separation

$$s = E(R^{1/4} - R^{-1/4}) \tag{8}$$

(Blandford & Kochanek 1987). Note that $R \sim 7$ for $s \sim E$.

3. PROBABILITY OF NONDETECTION FOR A POINT-MASS LENS

Consider a static point source at redshift z_s being doubly imaged by a single point lens at z_l . We derive the probability not to detect a secondary image with flux a factor $R > R_{\min}$ fainter than the bright image. Using equation (8), we see that failure to detect a secondary image places a lower bound on the source-lens angular separation

$$s > E(R_{\min}^{1/4} - R_{\min}^{-1/4}),$$
 (9)

where E depends on the lens and source redshifts. For a given source, there is then an excluded comoving volume for point masses of mass M, determined by the relation

$$V > V_{\min}(M) = R_0^3 \int \pi (s_{\min} r_{\text{com};l})^2 (1 - k r_{\text{com};l}^2)^{-1/2} dr_{\text{com};l}, \quad (10)$$

where $r_{\text{com};l}$ is the Robertson-Walker comoving coordinate of a lens (Weinberg 1972). We consider an Einstein-de Sitter universe, in which

$$r_{\text{com}}(z) = \frac{2c}{R_0 H_0} \left[1 - (1+z)^{-1/2} \right].$$
 (11)

In this case equation (10) evaluates to

$$V_{\min} = \frac{8\pi GM}{H_0^2} \left(R_{\min}^{1/4} - R_{\min}^{-1/4} \right)^2 \times \left[\frac{(1+z_s)^{1/2} + 1}{(1+z_s)^{1/2} - 1} \ln(1+z_s) - 4 \right]. \quad (12)$$

Nemiroff (1989) derived an equivalent expression and noted that, for a nearby source, the excluded volume has an ellipsoidal shape. Then equation (12) reduces to

$$V_{\min} = \frac{2\pi GM}{3H_0^2} \left(R^{1/4} - R^{-1/4} \right)^2 z_s^2 \,. \tag{13}$$

For larger source redshifts, the shape of the excluded volume becomes ovoid (Fig. 1).

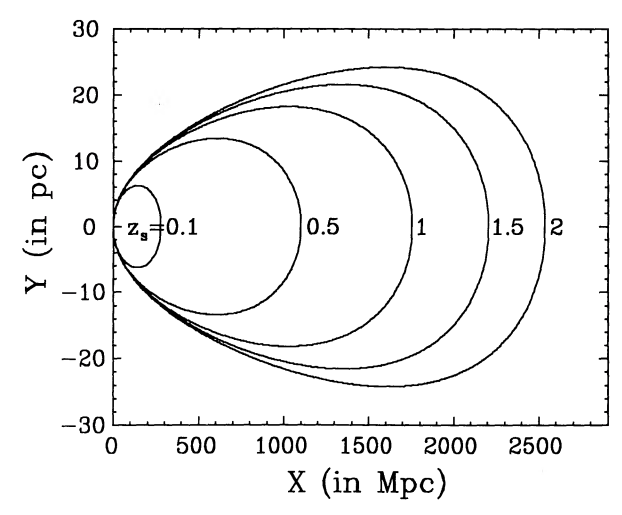


Fig. 1.—Cross sections of excluded volume for a point lens-point source system, in comoving coordinates, for several source redshifts. The mass of the lens is $10^6~M_{\odot}$, and the relative positions of lens and source are such that one image is at least 20 times brighter than the other ($R_{\rm min}=20$).

In addition to being too faint, secondary images can also be missed if they are unresolved. If the angular resolution is δ , then we will be able to detect only the presence of masses whose Einstein radii satisfy

$$x_{1, \min} - x_{2, \max} = x_{1, \min} + |x_{2, \max}|$$

$$= E(R_{\min}^{1/4} + R_{\min}^{-1/4}) > \delta$$
(14)

(Nemiroff 1989). This restriction places an effective lower bound on the mass range which can be explored. For a given mass, equation (14) is satisfied for all $z_l \le z_\delta$, where z_δ can be found from the solution of the cubic equation

$$T_{\delta}^{2} \frac{S - T_{\delta}}{T_{\delta} - 1} = \left(\frac{\delta}{R_{\min}^{1/4} - R_{\min}^{-1/4}}\right)^{2} \frac{c^{3}}{2GMH_{0}} (S - 1), \quad (15)$$

(with respect to T_{δ}), where

$$T_{\delta} = (1 + z_{\delta})^{1/2} , \qquad (16)$$

and

$$S = (1 + z_s)^{1/2} . (17)$$

There is a third restriction. We will only detect secondary images if they lie within the field of search of the observation, Δ . We must therefore stipulate that

$$E(R_{\min}^{1/4} + R_{\min}^{-1/4}) < \Delta$$
 (18)

This restriction imposes an effective upper bound on the mass range. For a given mass, this condition is satisfied for all $z_l \ge z_\Delta$, where z_Δ can be found from the solution of a cubic equation similar to equation (15), with Δ and

$$T_{\Lambda} = (1 + z_{\Lambda})^{1/2} \,, \tag{19}$$

in the place of δ and T_{δ} , respectively.

The angular resolution and field of search constraints result in that the excluded volume integral must be truncated at both ends. The truncated volume is

$$V_{t} = \frac{16\pi GM}{H_{0}^{2}} \left(R_{\min}^{1/4} - R_{\min}^{-1/4} \right)^{2} v(z_{s}, M, \delta, \Delta) , \qquad (20)$$

(27)

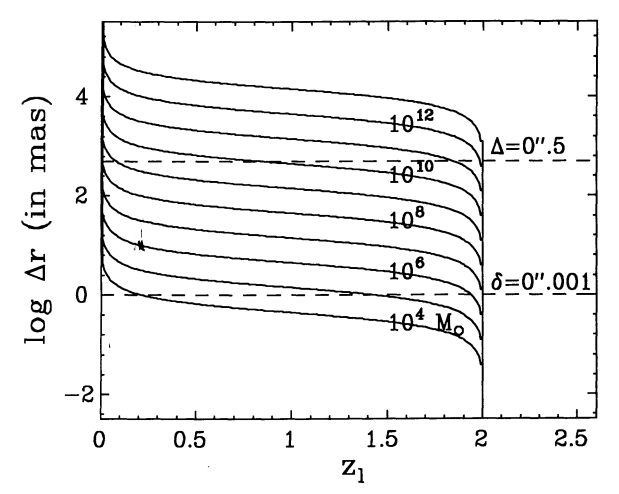


Fig. 2.—The angular separation (in mas) of the images as a function of the redshift of the lens, for a source at redshift $z_{\rm s}=2$. The mass of the lens ranges from 10^4 to $10^{13}~M_{\odot}$. The flux ratio of the images is R=20.

where we introduced a dimensionless volume function

$$\nu(z_s, M, \delta, \Delta) = \frac{S+1}{S-1} \ln \frac{T_{\delta}}{T_{\Delta}} - \frac{S}{S-1} \left(T_{\Delta}^{-1} - T_{\delta}^{-1} \right) - \frac{T_{\delta} - T_{\Delta}}{S-1} . \tag{21}$$

This function has an important property: when δ and Δ have values of practical interest, it depends only on the source redshift within a wide range of lens masses. In Figure 2 we have plotted the angular separation of the images against the redshift of the lens for several lens masses. It can be seen that for a point source at redshift $z_s=2$, imaged with R=20, $\delta\sim 1$ mas, and $\Delta\sim 0.75$, the upper truncation redshift is very close to the source redshift and the lower very close to zero within the mass range $10^6\lesssim M\lesssim 10^9~M_\odot$. Therefore truncation is negligible in this mass range, and the volume function ν can be considered independent of M. As the flux ratio R is increased, the masses at which the excluded volume is significantly reduced by the effects of finite angular resolution and field of search are decreased (Fig. 3). Note that these results are not particularly sensitive to the redshift of the point source.

We assume a uniform distribution of lenses in space, at uncorrelated positions. The compact lenses would, in general, have some spectrum of masses. However, let us first consider lenses of the same mass M, distributed with comoving density n_M . If Ω_M is their contribution to the average density of the universe, in units of the closure density, then

$$n_M = \frac{3H_0^2 \Omega_M}{8\pi GM} \,. \tag{22}$$

The expected number of compact objects within volume V_t is then simply $n_M V_t$. The probability of *failing* to detect one secondary image is given by the Poisson law

$$P_0 = e^{-n_M V_t}, (23)$$

where, taking into account equation (21), we find that

$$\ln P_0 = -6\Omega_M (R_{\min}^{1/4} - R_{\min}^{-1/4})^2 v(z_s, M, \delta, \Delta) . \tag{24}$$

Note that the probability of nondetection depends on the mass of the lens only through z_{δ} and z_{Δ} , that is, only when the angular separation of the images is taken into account (Press & Gunn 1973).

If we have observations of a large number of compact radio sources, and none of them has a secondary image, the total probability of nondetection is the product of the individual probabilities or, equivalently, equation (24) with V_t interpreted as the total excluded volume. We replace

$$v \to \sum_{i} v_i \,, \tag{25}$$

where i labels the compact radio sources.

Let us now consider compact objects with different masses, assuming

$$dn_M dV_{\text{com}} = \frac{3H_0^2}{8\pi GM} \frac{d\Omega_M}{dM} dM dV_{\text{com}}, \qquad (26)$$

objects of mass within interval (M, M + dM), in comoving volume $dV_{\rm com}$. Then the probability of nondetection of one object in this mass interval is given by the relation

$$\ln P_0 = -6(R_{\min}^{1/4} - R_{\min}^{-1/4})^2 \sum_i \int dM \, \frac{d\Omega_M}{dM} \, v(z_{s_i}, \, M, \, \delta, \, \Delta) \, .$$

In Figure 4a we have plotted $d \log P_0/d\Omega_M$ against the lens mass, for a sample of 48 compact radio sources (full details about the data used will be given in § 5). We see that $d \log P_0/d\Omega_M$ is roughly constant within the range $10^7 \lesssim M/M_\odot \lesssim 10^9$ and falls off sharply outside it. We can constrain the net cosmic density contributed by the masses within this range,

$$\Omega_{M}(10^{7}-10^{9} M_{\odot}) = \int_{10^{7} M_{\odot}}^{10^{9} M_{\odot}} \frac{d\Omega_{M}}{dM} dM,$$
(28)

from existing observations (§ 5).

In this section we considered the simplest approximation for lensing effects. A more sophisticated approach would take into account magnification bias: complete samples, constrained by flux thresholds, can be affected by magnification effects (Canizares 1981; Turner, Ostriker, & Gott 1984). Since the actual CRS samples are too small for very detailed statistics,

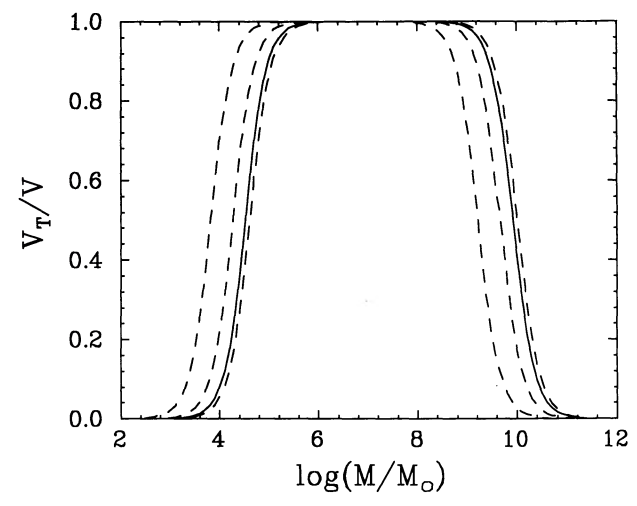
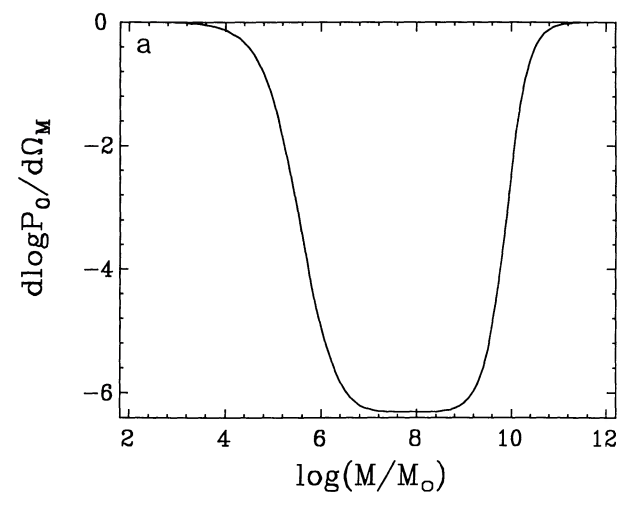


FIG. 3.—The ratio of the truncated to the total excluded volume, V_i/V , as a function of the mass of the lens, for four values of the minimal flux ratio: 10, 20, 100, and 1000 (the solid curve corresponds to R=20). The source is at redshift $z_s=2$, the angular resolution δ is 1 mas, and the field of search Δ is 0".5.



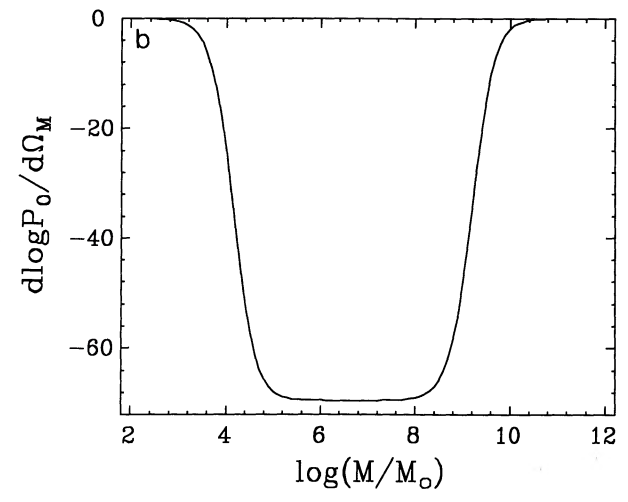


Fig. 4.—(a) $d \log P_0/d\Omega_M$ as a function of M, the mass of the lens, calculated from a sample of 48 CRS (§ 5). (b) $d \log P_0/d\Omega_M$ as a function of M, the mass of the lens, for a fictitious sample of 1000 CRS, observed with angular resolution $\delta = 0.5$ mas, dynamic range R = 1000 and field of view $\Delta = 0.5$.

we neglected this bias. There are also corrections for collective effects which we address in the next section.

4. COLLECTIVE EFFECTS BY COMPACT OBJECTS

In § 3, we neglected the fact that the mass contained in compact objects contributes to the overall mass density of the universe, so that the cosmography and in particular the geodesic deviation depend both on the amounts of mass in clumps and on mass smoothly distributed. If we compare two universes of the same average mass densities, one homogeneous and one clumpy, the backtracked light beams which start within the same (small) solid angle at the observer diverge by different amounts: beams passing between clumps in a clumpy universe diverge more than the beams in a homogeneous universe, and can thus be described by modified (larger) angular diameter distances (Zel'dovich 1964).

Press & Gunn (1973) addressed the Zel'dovich effect in the extreme case, in which all the mass of the universe is in clumps. Thus they profited by the coincidence between the affine parameter and the angular diameter distance in the case of an empty beam (no matter inside a beam). The same affine parameter was unfortunately used by Turner et al. (1984) in their treatment of point masses in an Einstein—de Sitter universe. By doing so, they neglected the extra focusing by matter inside the beam (nevertheless, they took the extra focusing into account in their treatment of isothermal spheres).

We address compact masses in a range limited by the resolution and by the field of search, $10^7 \lesssim M/M_\odot \lesssim 10^9$. Considering the convergence of light beams, we must regard the larger compact masses, $M \gg 10^9~M_\odot$ differently from the smaller masses, $M \ll 10^7~M_\odot$. The larger masses are to be treated the same as the masses within our range, as if, in effect, they contained matter taken away from the beams (Zel'dovich 1964). The smaller masses act on angular scales below our resolution; therefore, we regard them as included in the smooth matter inside the beam (Weinberg 1976).

For simplicity, we neglect in our evaluations the possibility of existence of the larger masses and assume cosmic density Ω_M in compact objects with masses within the range we address, and $1-\Omega_M$ smoothly distributed, in a universe with the Einstein-de Sitter global cosmography. The beams passing between the clumps can be addressed using distances derived

by Dyer & Roeder (1973): the angular diameter distance from redshift z_1 to redshift z_2 is

$$d_{12}^{DR} = \frac{2c}{H_0} \frac{1}{1+z_2} \frac{1}{\nu} \left[(1+z_1)^{-(\nu+1)} (1+z_2)^{(\nu-1)/4} - (1+z_2)^{-(\nu+1)/4} (1+z_1)^{(\nu-1)/4} \right]$$
(29)

where $v = (1 + 24\Omega_M)^{1/2}$ (Dyer & Roeder 1973).

We use the *balancing* of the lens equation proposed by Kovner (1989) for a clumpy universe, via the following approach: The lens equation is derived by comparing rays connecting the observer to some sources in the presence of lenses, with the same rays in the absence of lenses. Now comes an important point: we choose the absence of lenses to mean that the mass in clumps is smoothed out, and light travels in a homogeneous universe with the same overall density parameter. Therefore, for a point mass, we can write

$$d_{\text{os}}^{\text{IU}}s = d_{\text{os}}^{\text{DR}} \left(r - E_{\text{DR}}^2 \frac{r}{r^2} \right). \tag{30}$$

The left-hand side of the equation describes the propagation of light rays in absence of lenses, and therefore it involves angular diameter distances of an ideally isotropic universe, $d^{\rm IU}$. The right-hand side refers to a clumpy universe (presence of lenses), so $E_{\rm DR}$ is the Einstein radius calculated from equation (1) with Dyer-Roeder angular diameter distances.

For simplicity, we consider only the mass range $10^7 \lesssim M/M_\odot \lesssim 10^9$ and neglect the truncation of the excluded volume by the resolution and field of search constraints. We are going now to obtain an expression for the probability of failing to detect a compact mass in this range, the equivalent of equation (27) for a clumpy universe. We can determine the excluded volume from the relation

$$s > \frac{d_{\text{os}}^{\text{DR}}}{d_{\text{os}}^{\text{IU}}} E_{\text{DR}}(R^{1/4} - R^{-1/4})$$
 (31)

and calculate it from equations (10) and (11). Combining with equation (22), we find the expected number of compact objects of mass M inside the excluded volume and the probability of nondetection of a compact object of mass M:

$$\ln P_0 = -3\Omega_M (R^{1/4} - R^{-1/4})^2 \mathscr{F}(\Omega_M, z_s)$$
 (32)

where

$$\mathscr{F} = \frac{1}{\nu} \frac{\sqrt{1+z_s} [1-(1+z_s)^{-\nu/2}]}{(\sqrt{1+z_s}-1)^2} \times \int_0^{z_s} \frac{(\sqrt{1+z}-1)^2}{(1+z)^{3/2}} \frac{(1+z_s)^{\nu/2}-(1+z)^{\nu/2}}{(1+z)^{\nu/2}-1}, \quad (33)$$

while the probability to detect a compact object in the mass range $10^7 \lesssim M/M_{\odot} \lesssim 10^9$ is given by

$$\ln P_0 = -3(R^{1/4} - R^{-1/4})^2 \sum_i \int dM \, \frac{d\Omega_M}{dM} \, \mathscr{F}(\Omega_M, z_s) \,, \quad (34)$$

where Ω_M is the collective fractional density given by equation (28).

In the limit $\Omega_M \to 0$, the probability given by equations (32) and (33) goes to equation (12) (cf. Nemiroff [1989] for the probability in the $\Omega_M \to 0$ limit, which is equivalent to our equation [12]). Taking into account the Zel'dovich effect on light beams passing between clumps yields larger excluded volumes, therefore smaller nondetection probabilities and lower bounds on Ω_M .

We have neglected other collective effects by compact masses. In particular, the action of a particular point mass can be affected by other point masses which happen to be near the light rays involved. The multiple scattering contributes to the distortion and magnification of images; however, it is statistically rare for small Ω_M (Press & Gunn 1973).

5. VLBI OBSERVATIONS OF COMPACT RADIO SOURCES

Let us now turn to the observations. A VLBI map of a compact radio source is characterized by its dynamic range, the ratio of the brightness of the brightest feature in the map to the rms noise in an area of blank sky (Pearson & Readhead 1988). Frequently, in maps of compact radio sources, the brightest feature is an unresolved or barely resolved core component. If this is multiple-imaged and no secondary counterpart is seen, then we can use the dynamic range to estimate a lower bound on R, the flux magnification ratio associated with the closest point mass: a secondary image will not be detected unless its flux is larger than 2-3 times the noise level; therefore, in case of nondetection, R should be larger than one-third of the dynamic range of the map.

The quoted dynamic ranges of published VLBI maps range from ~ 10 to a current maximum value of $\sim 3 \times 10^3$ in 3C 345 (Wehrle & Unwin 1991). A fully configured VLBI, perhaps linked with a global network, can aspire to a dynamic range $R \sim 10^5$ in the strongest sources, comparable with the best currently achievable with the VLA (Wilkinson 1987), though a value closer too $\sim 10^4$ is more realistic for a large sample. As can be seen from equation (27), the density limits depend upon the mean square root dynamic range and the most stringent limits (and also the best prospects for detecting an intergalactic compact object) involve the more numerous, lower flux sources that are observed with more modest dynamic range.

The typical field of search of VLBI maps is $\gtrsim 1''$ (T. J. Pearson, private communication). Lower resolution maps, e.g., those made with VLA, can be searched as well for compact objects. It is unlikely that extra point sources would not have been reported at separations between 10^{-3} arcsec and 1". Galaxies are responsible for observed multiple images with angular separations $\gtrsim 1''$, and these can also be sought opti-

TABLE 1
OBSERVATIONAL DATA ON SUPERLUMINAL RADIO SOURCES

Object	z	δ (mas)	References
3C 120	0.033	7	1
NRAO 140	1.258	0.5	2
3C 395	0.635	3	3
3C 390.3	0.0569	1	4
1928 + 738	0.302	1	5
1642 + 690	0.751	1	6
0850 + 581	1.322	1.5	6
1150+812	1.25	1	5
3C 216	0.669	1.2	6
3C 245	1.029	2.04	7
4C 34.47	0.206	2	8
$0735 + 178 \dots$	0.424	1.5	9
OJ 287	0.306	6.5	10
0212 + 735	2.367	0.8	5
3C 279	0.538	3.2	11
3C 273	0.158	0.6	12
3C 345	0.595	0.55	13
BL Lac	0.070	0.75	14
4C 39.25	0.699	0.73	15
3C 454.3	0.859	2	16
3C 263	0.652	0.35	7
1951 + 498	0.466	0.2	17
CTA 102	1.037	5	18

REFERENCES.—(1) Walker et al. 1987; (2) Marcher & Broderick 1985; (3) Simon et al. 1987; (4) Alef et al. 1988; (5) Witzel 1987; (6) Pearson et al. 1987; (7) Hough & Readhead 1987; (8) Barthel 1987; (9) Baath 1984; (10) Roberts & Wardle 1987; (11) Unwin 1987; (12) Cohen et al. 1987; (13) Wehrle & Unwin 1991; (14) Phillips & Mutel 1982; (15) Shaffer & Marcher 1987; (16) Pauliny-Toth 1987; (17) Zensus & Porcas 1986; (18) Baath 1987.

cally (cf. Turner et al. 1984; see Crampton et al. 1989 for a report on a specific search for closely spaced quasar images).

We have considered two samples of compact radio sources. The first comprises 23 out of the 24 currently known superluminal radio sources (Porcas 1987). We could not find usable data for the remaining source. In Table 1 we list the 23 sources together with their redshifts and angular resolutions. We also used a part of the Pearson-Readhead sample (Pearson & Readhead 1988). Out of the 37 objects listed in their Table 3, we removed all superluminal sources (included in our first sample) and all sources, for which redshifts were not available. This left 25 objects, for which data are given in Table 2.

Note that the angular resolution of the observations, defined as the FWHM of the restoring beam, is not the same in every direction: the FWHM contours are usually elliptical. In all cases we adopt the value of the major axis of the ellipse as angular resolution.

Dynamic ranges and fields of view were not explicitly given for any of the objects in the two samples. Pearson & Readhead give a collective dynamic range of 50–300 for all their maps. The dynamic range of the SRS maps should be at least of the same order of magnitude (Pearson & Zensus 1987). We adopted R=20 and $\Delta=0.5$ for all objects. It should be noted, however, that the results of this analysis are not very sensitive to the particular values of R and Δ .

Some of the sources in both samples are classified as very compact, while others have parsec-scale extended emission. In most of the latter cases, the extended components have been identified as jets and have steeper radio spectra and higher polarization than the bright core (Pearson & Readhead 1988). In some cases, however, the weaker components are so close to the bright cores that it is difficult to study their spectral, polar-

TABLE 2

OBSERVATIONAL DATA ON THE PEARSON-READHEAD SAMPLE

Object	z	δ(mas)
0016+731	1.781	1.8
0133 + 476	0.859	4
0153 + 744	2.338	1.5
0316+413	0.0172	2.8
0710+439	0.518	1.4
0711 + 356	1.62	1.8
0804 + 499	1.43	1.3
0831 + 557	0.242	2
0836 + 710	2.17	1.3
0859 + 470	1.462	2.9
0945 + 408	1.252	2.9
1458 + 718	0.905	1.3
1624 + 416	2.55	1.8
1633 + 382	1.814	1.8
1637 + 574	0.745	2.7
1652 + 398	0.0337	1.9
1739 + 522	1.375	1.1
1803 + 784	0.68	1.1
1807 + 698	0.05	2.8
1823 + 568	0.664	1.1
1828 + 487	0.696	2.9
1954 + 513	1.22	2.9
2021 + 614	0.2266	2
2351 + 456	2	3.8
2352+495	0.237	1.4

ization, and variability properties, and therefore to understand whether they are extended emission features or secondary images. It is also suspected that very weak extensions may not be real: they are the sort of features that could be created by the imaging process, if the source varied during the observation (T. J. Pearson, private communication). We simulated the case of a weak component (Figs. 5 and 6) by taking two Gaussian brightness distributions, one of them 20 times brighter than the other, with identical FWHM = δ , at gradually increasing distance from each other. At close distances (Figs. 5a-5d and 6a-6d), the two components are not clearly separated, but at a

distance of 2δ (Figs. 5e and 6e) they can be considered distinguishable, so that it is possible to study the properties (spectrum, polarization, variability) of each of them separately.

In order to take this fact into account, we have used in our calculations an effective angular resolution of 2δ , that is, twice the value given for each source in Tables 1 and 2.

The Pearson-Readhead sample contains five sources classified as "compact double" (cf. Phillips & Mutel 1982). The superluminal source 4C 39.25 is also a member of the same class. One might tend to consider these sources as candidate multiple-imaged sources (cf. Burke 1990). These particular sources, however, are morphologically different from all other types of compact radio sources in the sample: they are reported to exhibit low polarization and little variability, and they have no prominent large-scale structure (cf. Pearson & Readhead 1988). All these properties should be unaffected by a gravitational lens. Any compact double source that is not morphologically different is a prima facie candidate for gravitational lensing.

For both samples, we have combined the redshifts, angular resolutions, and estimated dynamic ranges to derive nondetection probabilities using equations (27) and (34). If we wish to reject the hypothesis that the universe is filled with compact objects in the mass range $10^7 \lesssim M/M_\odot \lesssim 10^9$ to a fraction $\Omega_{\rm min}(M)$ of the critical density at the $100\Pi\%$ confidence level, the following condition must be valid:

$$\left(\frac{d \log P_0}{d\Omega_M}\right)_{10^7 < M/M_{\odot} < 10^9} \Omega_{\lim} < \log (1 - \Pi) .$$
 (35)

In Figure 7, we quote 99.7% upper limits on $\Omega_M(M)$, for the simple approximation of § 3, and for the more sophisticated approximation of § 4. We see that the difference between these approximations can be appreciable only in the case of a large cosmological density of compact objects, which is already excluded. In Figure 8 we give similar results for a hypothetical survey of 1000 sources mapped uniformly with dynamic range R = 1000, field of search $\Delta = 0.5$, and angular resolution

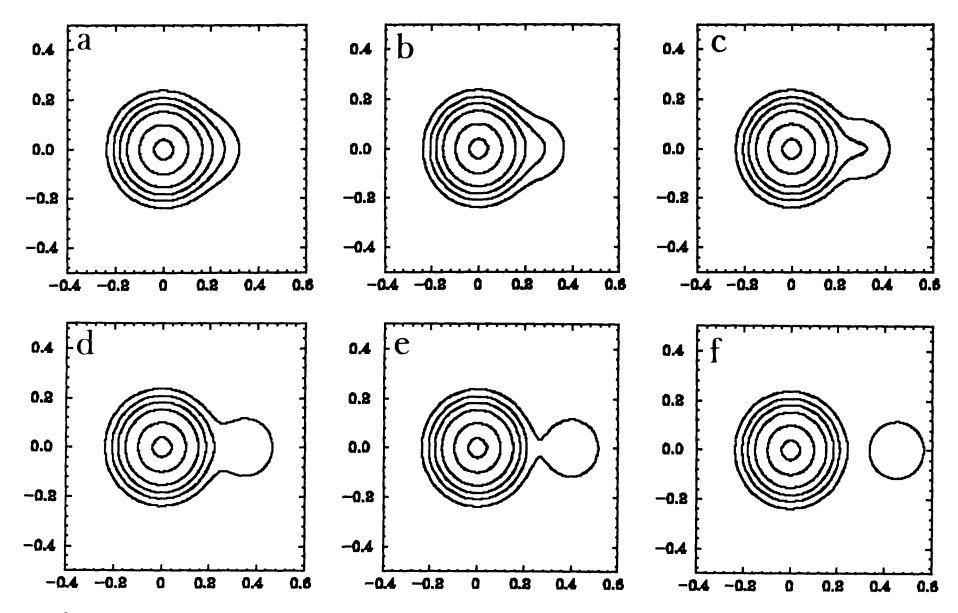


FIG. 5.—Isodensity contours for two Gaussian brightness distributions, one of them 20 times brighter than the other, at distances equal to (a) 0.20, (b) 0.25, (c) 0.30, (d) 0.35, (e) 0.40, and (f) 0.45 (arbitrary units). The FWHM of both distributions is 0.2 in the same units. The contour levels are 90, 50, 20, 10, 5, and 2% of the peak brightness.

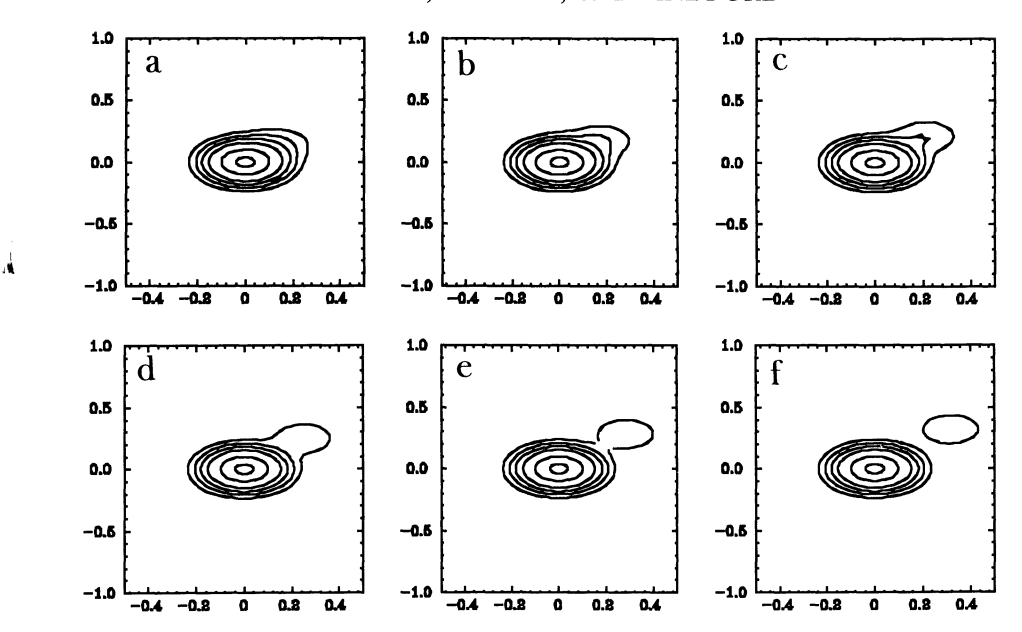


Fig. 6.—The same isodensity contours, elliptically distorted

 $\delta=0.5$ mas. In this case the effective resolution is $3\delta=1.5$ mas, and the mass range explored $10^5 \lesssim M/M_{\odot} \lesssim 10^8$ (from Fig. 4b).

If such a search is performed routinely using VLBI observations, it will be necessary to quote fields of view and upper limits on the flux ratio of any isolated compact source relative to the total observed flux. For sources with large achievable dynamic range, any faint, secondary source will be, at best, only partially resolved. However, given a hypothetical secondary source location, it is possible to predict both the expected spectrum and polarization from observations of the primary image. These two properties can be used to decide whether or not it is a gravitational lens image.

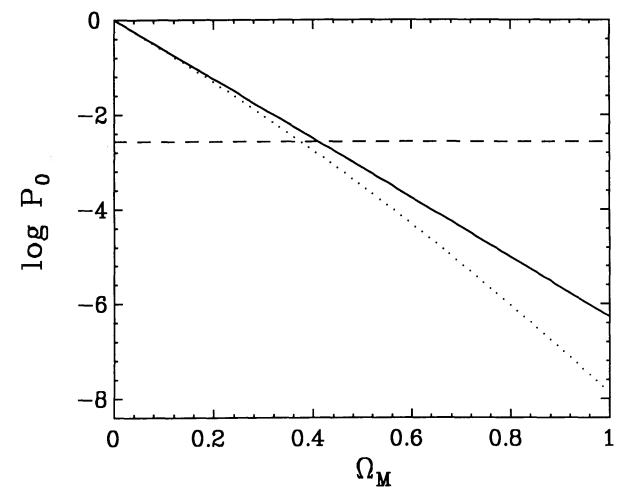


Fig. 7.—Total probability of nondetection for a point lens in the mass range 10^7 – $10^9~M_{\odot}$ in an Einstein–de Sitter universe, against the fractional density in lenses Ω_{M} , calculated from eqs. (27) (solid line) and (34) (dotted curve), from 48 CRS with dynamic range R=20 and field of view $\Delta=0.75$. The point of intersection of the probability curves with the dashed line give 99.7% limits on Ω_{M} .

6. DISCUSSION

In this paper, we have considered the use of observations of compact radio sources for setting limits on the density of intergalactic compact objects. We have shown that, by adopting a conservative estimate of the dynamic range of published maps and making simplifying assumptions about the source structure, we can set interesting upper limits on the cosmological density parameter for masses in the range $10^7 \lesssim M/M_\odot \lesssim 10^9$ of $\Omega \lesssim 4 \times 10^{-1}$. We believe that a reexamination of the whole VLBI archive would lead to a slight reduction of this lower bound.

However, and this is the main point of this paper, the prospects for setting a significantly lower bound, or conversely actually finding evidence for a population of compact objects, are very good. It should be a relatively simple procedure to

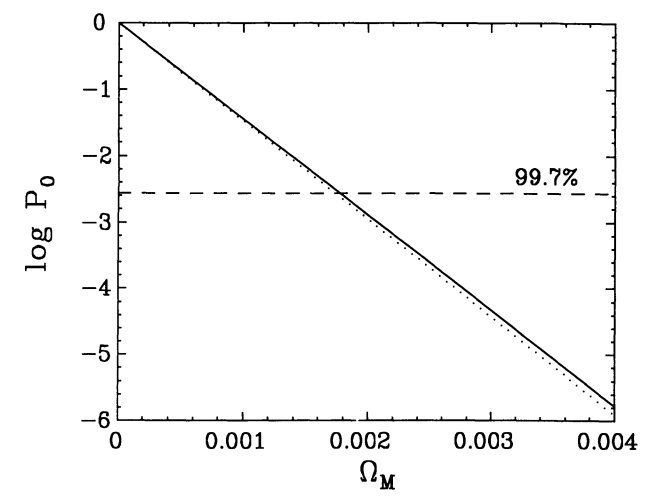


Fig. 8.—Same as Fig. 7, for a fictitious sample of 1000 CRS, observed with angular resolution $\delta = 0.5$ mas, dynamic range R = 1000, and field of view $\Delta = 0.5$.

scrutinize maps produced under relatively uniform conditions during VLBI surveys using the VLBI and the European VLBI Network (EVN) to quote upper limits on inverted demagnified images within the field of view. (The Southern Hemisphere survey [Preston et al. 1989], should also be useful in this respect.)

Assuming that 1000 high-redshift sources will ultimately be mapped with a typical dynamic range of $\sim 10^3$, we estimate that the upper bound on the density parameter of intergalactic compact objects in the mass range $10^5-10^8~M_{\odot}$ could be lowered to $\sim 10^{-3}$. In view of the possibility that a first generation of massive objects formed prior to galaxies and evolved

to form black holes in this mass range, this search is well motivated.

We thank J. Hewitt, C. Kochanek, R. Nemiroff, T. Pearson, R. Perley, A. Readhead, S. Unwin, and A. Wehrle for helpful advice. This research was supported in part by a NATO doctoral grant, administered by the Greek Ministry of National Finance, the United States-Israel Binational Science Foundation grant 88-00461, the funds granted by the Charles H. Revson Foundation, National Science Foundation grant AST 89-15326, and NASA grant NAGW 1301.

REFERENCES

(Cambridge: Cambridge Univ. Press), 206
Barthel, P. D. 1987, in Superluminal Radio Sources, ed. J. A. Zensus & T. J. Pearson (Cambridge: Cambridge Univ. Press), 148
Barnothy, J. M. 1982, in IAU Symposium 97, Extragalactic Radio Sources, ed. D. S. Heeschen & C. M. Wade (Dordrecht: Reidel), 463

Blandford, R. D., & Jaroszyński, M. 1981, ApJ, 246, 1

Blandford, R. D., & Kochanek, C. S. 1987, in Dark Matter in the Universe, ed. J. Bahcall, T. Piran, & S. Weinberg (Singapore: World Scientific), 133

Burke, B. F. 1990, in Proc. of the Toulouse Workshop on Gravitational Lensing, ed. Y. Mellier, B. Fort, & G. Soucail (Berlin: Springer), 127

Canizares, C. R. 1981, Nature, 291, 620

. 1982, ApJ, 263, 508

Cohen, M. H., Zensus, J. A., Biretta, J. A., Comoretto, G., Kaufmann, P., & Abraham, Z. 1987, ApJ, 315, L89
Crampton, D., McClure, R. D., Fletcher, J. M., & Hutchings, J. B. 1989, AJ, 98,

Dyer, C. C., & Roeder, R. C. 1973, ApJ, 180, L31
Hough, D. H., & Readhead, A. C. S. 1987, in Superluminal Radio Sources, ed. J. A. Zensus & T. J. Pearson (Cambridge: Cambridge Univ. Press), 114
Hewitt, J. N., Burke, B. F., Turner, E. L., Schneider, D. P., Lawrence, C. R., Langston, G. I., & Brody, J. P. 1989, in Gravitational Lenses, ed. J. M. Moran, J. N. Hewitt, & K. Y. Lo (Berlin: Springer), 147

Kovner, I. 1989, ApJ, submitted

Marcher, A. P., & Broderick, J. J. 1985, ApJ, 290, 735 Nemiroff, R. J. 1989, ApJ, 341, 579

——. 1991, Phys. Rev. Letters, 66, 538 Ostriker, J. P., & Vietri, M. 1985, 318, 446

Pauliny-Toth, I. I. K. 1987, in Superluminal Radio Sources, ed. J. A. Zensus & T. J. Pearson (Cambridge: Cambridge Univ. Press), 55
Pearson, T. J., & Readhead, A. C. S. 1988, ApJ, 328, 114

Pearson, T. J., Readhead, C. S., & Barthel, P. D. 1987, in Superluminal Radio Sources, ed. J. A. Zensus & T. J. Pearson (Cambridge: Cambridge Univ.

Pearson, T. J., & Zensus, J. A. 1987, in Superluminal Radio Sources, ed. J. A.

Zensus & T. J. Pearson (Cambridge: Cambridge Univ. Press), 1 Phillips, R. B., & Mutel, R. L. 1982, ApJ, 257, L19 Porcas, R. W. 1987, in Superluminal Radio Sources, ed. J. A. Zensus & T. J. Pearson (Cambridge: Cambridge Univ. Press), 12 Press, W. H., & Gunn, J. E. 1973, ApJ, 185, 397

Preston, R. A., et al. 1989, AJ, 98, 1
Roberts, D. H., & Wardle, J. F. C. 1987, in Superluminal Radio Sources, ed.
J. A. Zensus & T. J. Pearson (Cambridge: Cambridge Univ. Press), 193
Simon, R. S., Johnston, K. J., Hall, J., Spencer, J. H., & Waak, J. A. 1987, in Superluminal Radio Sources, ed. J. A. Zensus & T. J. Pearson (Cambridge: Cambridge Living Press), 22 Cambridge Univ. Press), 72 Turner, E. L., Ostriker, J. P., & Gott, J. R. 1984, ApJ, 284, 1 Unwin, S. C. 1987, in Superluminal Radio Sources, ed. J. A. Zensus & T. J.

Pearson (Cambridge: Cambridge Univ. Press), 34
Walker, R. C., Benson, J. M., & Unwin, S. C. 1987, in Superluminal Radio Sources, ed. J. A. Zensus & T. J. Pearson (Cambridge: Cambridge Univ. Press), 48

Wehrle, A., & Unwin, S. C. 1991, in IAU Symposium 131, Radio Interferometry, Theory, Techniques and Applications, ed. T. Cornwell (Dordrecht:

Pearson (Cambridge: Cambridge Univ. Press), 211

Zel'dovich, Ya. B. 1964, Astr. Zh., 41, 19 (Soviet Astr., 8, 13) Zensus, J. A., & Porcas, R. W. 1986, in IAU Symposium 119, Quasars, ed. G. Swarup & V. K. Kapahi (Dordrecht: Reidel), 167